Morphology Development in Isotactic Polypropylene/Partially Hydrogenated Oligo(styrene-*co*-indene) Blend

Chang Hyung Lee, Hiromu Saito, and Takashi Inoue*

Department of Organic and Polymeric Materials, Tokyo Institute of Technology, Ookayama, Meguro-ku,Tokyo 152, Japan

Received June 13, 1995; Revised Manuscript Received August 21, 1995[⊗]

ABSTRACT: We investigated the spherulite formation in an isotactic polypropylene (iPP)/partially hydrogenated oligo(styrene-*co*-indene) blend by time-resolved light scattering equipped with a CCD camera system and transmission electron microscopy (TEM). The V_v (parallel polarization) light scattering pattern at a high crystallization temperature (T_c = 105 °C) changed from a single-ring pattern to a double-ring one and then to a circular symmetric one. Based on model calculation, the formation of the ring pattern can be interpreted by the positive birefringence spherulite which is expected to appear when the crosshatched lamellae sufficiently develop. The H_v (cross-polarization) light scattering pattern was the rod type, implying that a high level of orientation ordering was established in radial direction but a low level in tangential one. It is consistent with the above argument on the V_v patterns since the less ordering in tangential orientation could be caused by the crosshatching. Similar analysis on the crystallization at a low temperature (T_c = 85 °C) showed a formation of noncrosshatched and fragmented lamellae. The analysis was supported by the TEM observation. Thus, we found that the new morphologies are available by adding miscible impurity and controlling the T_c.

Introduction

It is well-known that the spherulite of isotactic polypropylene (iPP) consists of crosshatched lamella branching; i.e., subsidiary lamellae grow tangentially to the radiating primary lamellae.[1] The fraction of crosshatch lamellae in iPP spherulites is high at a low crystallization temperature T_c, and it decreases with increasing T_c.[2] When the fraction of crosshatch lamellae is sufficiently high, the radial refractive index of the spherulite is higher than the tangential one; i.e., the birefringence of the spherulite becomes positive.[2] On the other hand, the birefringence is negative when the fraction of radial lamellae is high. Hence, the birefringence changes the sign from positive to negative with increasing T_c.[2]

Recently, we found that iPP and a partially hydrogenated oligo(styrene-*co*-indene) (HSI) are miscible above the melting temperature of iPP. The iPP/HSI blend provides a nice opportunity to investigate the effect of miscible impurity on spherulite formation. In this paper, we carry out time-resolved light scattering studies on the spherulite formation at various T_c's using a highly sensitive charge-coupled device (CCD) camera system. The results are assessed by transmission electron microscopy (TEM).

Experimental Section

The iPP used was a commercial polymer supplied by Mitsui Toatsu Chemicals, Inc. (J3HG; M_w = 3.5 × 10^5, M_n = 5.0 × 10^4). HSI was obtained from Arakawa Chemicals, Ltd. (Arkon; M_w = 770).

iPP and HSI were melt-mixed at 190 °C using a Mini Max Moulder (CS-183 MMX, Custom Scientific Instruments, Inc.). The blend ratio was fixed at a 30/70 (iPP/HSI) weight ratio. The single-phase melt was extruded and chopped into pellets. A thin-layer specimen (~15 μm thick) was prepared by pressing the pellets between two cover glasses at 200 °C.

After the specimen was held at 200 °C for 3 min, it was rapidly transferred into a light scattering hot stage set at the desired crystallization temperature. The light scattering apparatus is shown schematically in Figure 1.[3] A polarized He−Ne gas laser of 632.8-nm wavelength was applied vertically to the film specimen. The scattered light was passed through an analyzer. We employed two optical geometries; one was the H_v geometry in which the optical axis of the analyzer was set perpendicularly to that of the polarizer, and the other was the V_v geometry with a parallel set of the two axes. The angular distribution of light scattering intensity was detected by a highly sensitive CCD camera with 576 × 382 pixels (Princeton Instruments, Inc.).

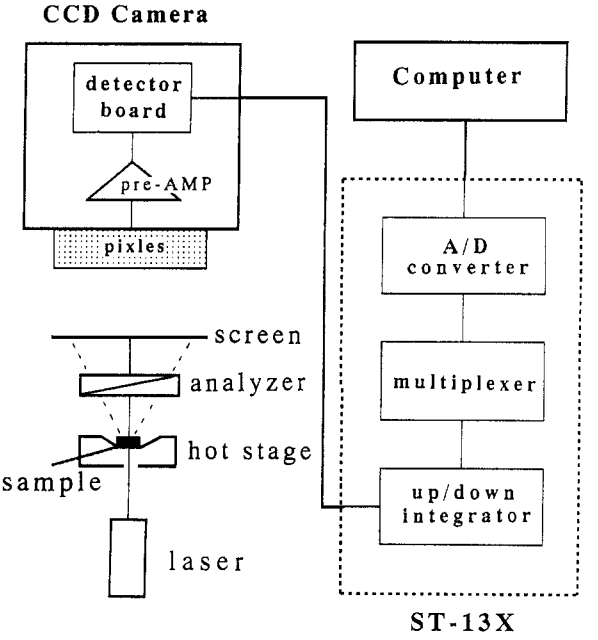

Figure 1. Light scattering apparatus.

Structural development during the isothermal crystallization was also observed under polarized optical microscope with a sensitive tint plate (Olympus BH-2).

For TEM analysis, ultrathin sections were cut with microtome from crystallized samples and stained with ruthenium tetraoxide (RuO_4) in the gas phase. The lamellar morphology was observed under TEM with an accelerator voltage of 100 kV (JEM-100CX, JEOL Ltd.).

* To whom correspondence should be addressed.

[⊗] Abstract published in *Advance ACS Abstracts,* October 15, 1995.

0024-9297/95/2228-8096$09.00/0

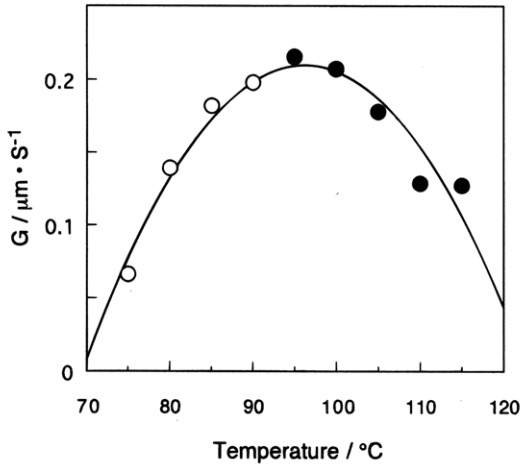

Figure 2. Temperature dependence of the growth rate in a 30/70 iPP/HSI blend: (●) positive birefringence spherulite and (○) negative birefringence spherulite by optical microscopy.

Results and Discussion

Figure 2 shows the crystallization temperature (T_c) dependence of the crystallization growth rate (G) in the 30/70 iPP/HSI. Note here that the G was obtained by the slope of the time variation of the spherulite radius. The radius at high crystallization temperatures (T_c > 95 °C) was obtained by the peak maximum of the V_v scattering profile (see eq 6) and that at low temperature was by the peak of the H_v scattering pattern (see eq 10). G increases with increasing T_c and attains a maximum at T_{max} = 95 °C. Morphology evolution was found to be different below and above 95 °C. Hence, in this paper, we will confine discussion to two representative temperatures; i.e., one is 105 °C ($T_c > T_{max}$) and another is 85 °C ($T_c < T_{max}$).

Figure 3 shows the change in the V_v and H_v scattering patterns during the crystallization at T_c = 105 °C. In Figure 3 is also shown the time variation of the integrated scattering intensity, the invariant Q:

$$Q = \int_0^\infty I(q) q^2 \, dq \tag{1}$$

where $I(q)$ is the intensity of the scattered light at the scattering vector q, $q = (4\pi/\lambda)/\sin(\theta/2)$, λ and θ being the wavelength and scattering angle, respectively.[4] The invariant in H_v mode, Q_{H_v}, is described by the mean-square optical anisotropy $\langle\delta^2\rangle$

$$Q_{H_v} \propto \langle\delta^2\rangle = \phi_s(\alpha_r - \alpha_t)^2 \tag{2}$$

where ϕ_s is the volume fraction of spherulites and α_r and α_t are the radial and tangential polarizabilities of the spherulite, respectively. The invariant in the V_v mode, Q_{V_v}, is ascribed to both $\langle\delta^2\rangle$ and the mean-square density fluctuation $\langle\eta^2\rangle$. The $\langle\eta^2\rangle$ is given by

$$\langle\eta^2\rangle = \phi_s(1 - \phi_s)(\alpha_s - \alpha_0)^2 \tag{3}$$

where α_s is the average polarizability of the spherulite and α_0 is the polarizability of the melt. Hence, the Q_{H_v} is expected to increase with increasing volume fraction of spherulites and then level off when the spherulites are volume-filled, while the Q_{V_v} is expected to attain a maximum when the spherulites occupy 50% volume. Such time variations in Q_{H_v} and Q_{V_v} are seen in Figure 3. It is also seen in Figure 3 that the onset time of invariant $Q_{H_v}(t_{OH})$ is different from that of $Q_{V_v}(t_{OV})$. The

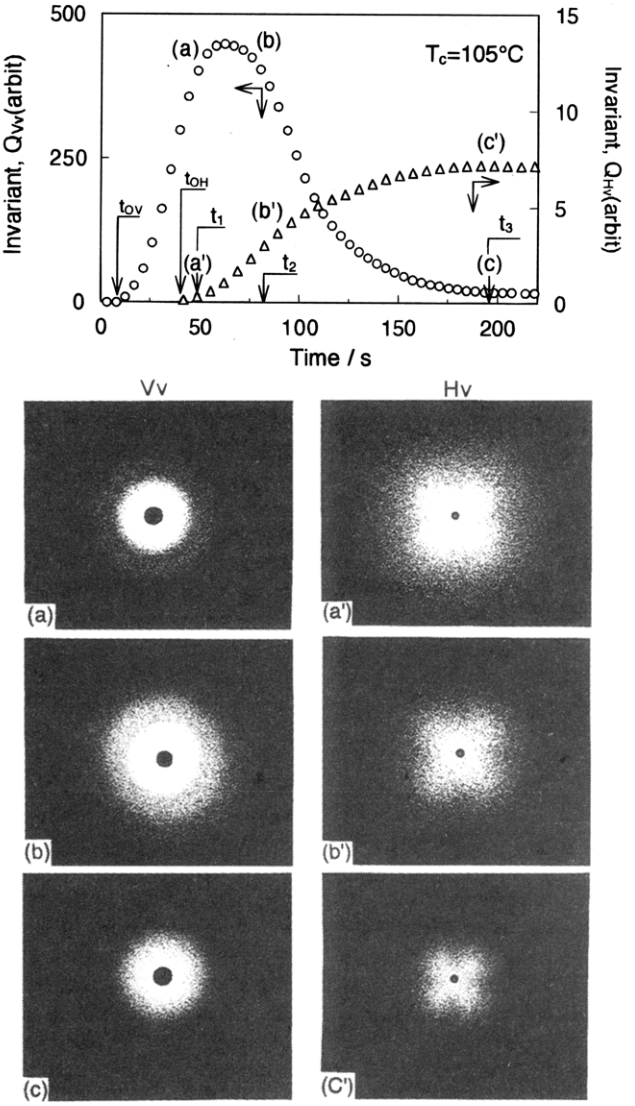

Figure 3. Changes in the invariant and the scattering patterns, both under H_v and V_v modes: 30/70 iPP/HSI blend, T_c = 105 °C. (a, a′) 50, (b, b′) 80, and (c, c′) 190 s.

time lag ($t_{OV} - t_{OH}$) is ascribed to the development of an isotropic domain as the precursor of the spherulite, as discussed in our previous paper.[3] The V_v scattering patterns observed at three crystallization times (t_1, t_2, and t_3) are shown by panels a–c in Figure 3. Corresponding H_v patterns are shown in panels a′–c′.

In V_v mode, a single-ring pattern appears at an early stage of crystallization (a) and then another ring appears at wide angle (b). That is, the V_v pattern changes from single ring to double ring with time of crystallization. The rings become smaller with time. Finally, the rings disappear and a weak circular symmetric pattern is observed after the spherulites have volume-filled (c). In H_v mode, the rod-type pattern (a′) is observed and it becomes smaller with time (b′, c′).

The V_v scattering pattern is theoretically described by[5,6]

$$I_{V_v} = AV^2 \cos^2 \varrho_1 (3/U^3)^2 \{(\alpha_r - \alpha_s)(\mathrm{Si}\, U - \sin U) + (\alpha_t - \alpha_s)(2 \sin U - U \cos U - \mathrm{Si}\, U) + (\alpha_r - \alpha_t)[\cos^2(\theta/2)/\cos\theta]\cos^2\mu(4 \sin U - U \cos U - 3\, \mathrm{Si}\, U)\}^2 \tag{4}$$

$$\cos^2 \varrho_1 = \cos\theta/(\cos^2\theta + \sin^2\theta \cos^2\mu)^{1/2} \tag{5}$$

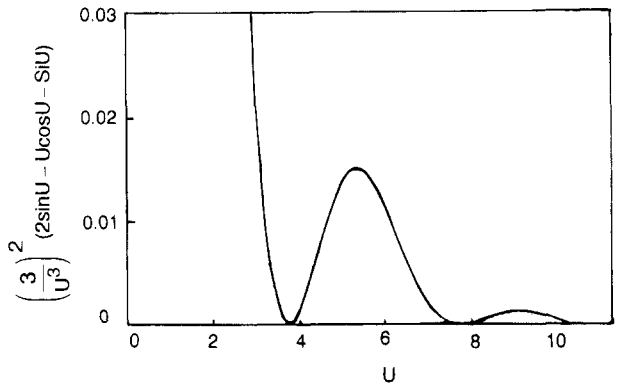

Figure 4. The second term in eq 4 (calculated).

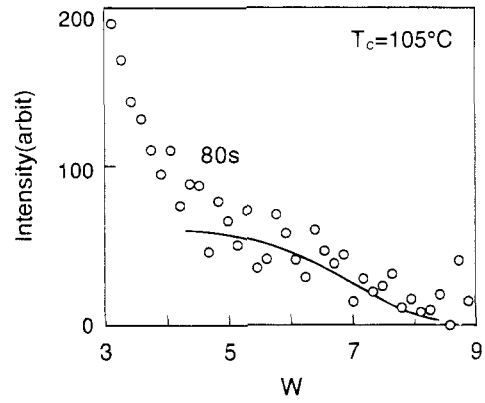

Figure 5. H_v scattering intensity as a function of w. The solid line is a curve calculated by eq 8, setting a = 2.2 μm: 30/70 iPP/HSI blend crystallized at T_c = 105 °C for 80 s.

where A is a proportionality factor, V is the volume of spherulites of radius R_s, μ is the azimuthal angle, and α_s is the polarizability of the surroundings. Si U is the sine integral defined as

$$\text{Si } U = \int_0^U \frac{\sin x}{x}\, dx$$

where U is given by

$$U = 4\pi(R_s/\lambda)\sin(\theta/2) \qquad (6)$$

The single-ring pattern in V_v mode at the early stage of crystallization suggests that the third term of eq 4 is minor so that there is no azimuthal angle dependence in the V_v pattern. This may be caused by $\alpha_r \approx \alpha_t$. By numerical calculation, one can show that the first term in eq 4 is very small, two decades smaller than the second term, when α_r is comparable to α_t. In Figure 4 is shown the calculated curve of the second term of eq 4, $\{(3/U^3)^2(2 \sin U - U \cos U - \text{Si } U)\}$, as a function of U. It has two maxima at U = 5.7 and 9.0. Setting the U = 5.7 and using the peak angle in Figure 3a,b, the spherulite radius R_s was estimated by eq 6. The estimated values R_s were exactly equal to those obtained by the optical microscopic observation.

The spherulites with weak positive birefringence were observed under the polarized microscopy at early stage. It suggests $\alpha_r \geq \alpha_t$. The birefringence of a spherulite is given by[6]

$$\Delta n = n_r - n_t = ((3f - 1)/2)(n_c - n_a) \qquad (7)$$

where f is the fraction of crosshatch lamellae. n_c and n_a are the principal refractive indexes along the a- and c-axes of a crystal, respectively. The weak positive birefringence ($\Delta n \geq 0$) suggests that f is slightly larger than 1/3, implying a significant amount of the crosshatch lamellae. The Δn increases with increasing the fraction of crosshatch lamellae. Since Δn is proportional to $\alpha_r - \alpha_t$, the value of $\alpha_r - \alpha_t$ increases with increasing fraction of crosshatch lamellae. The intensity of the second peak at U = 9.0 in Figure 4 becomes larger with increasing $\alpha_r - \alpha_t$. This may render the change in pattern from single ring to double ring during the crystallization, as shown in Figure 3a,b. The peak shifts to smaller angle with increasing R_s, then approaches 0°, and the ring pattern disappears, as shown in Figure 3c.

As shown in Figures 3a′−c′, the H_v pattern is the rod-type and it becomes smaller with time. However, rodlike aggregates were not obvious under the polarized microscope, but spherulites with a diffuse maltese cross pattern were observed. According to Stein and Chu,[7] the relative intensity of scattered light from a spherulite at angles less than the scattering maximum ($\theta < \theta_{max}$) is enhanced by the disorder in the tangential direction, whereas the relative intensity at the wide-angle region ($\theta > \theta_{max}$) is enhanced by the disorder in the radial direction. Thus, the appearance of the rodlike pattern in the H_v mode may be caused by the excess intensity at the small angles due to a low level of orientation ordering in the tangential direction and a high level in the radial direction. Less ordering in the tangential orientation in the spherulite could be caused by the orientational disorder of the crosshatch. The ordering in the radial direction can be analyzed quantitatively in terms of scattering variables as follows.

A typical one-dimensional H_v scattering profile at μ = 45° is shown by the open circles in Figure 5. The H_v intensity decreases monotonously with the reduced angle parameter w, defined by $(2\pi/\lambda)R_s \sin\theta$, R_s being calculated from the peak in the V_v profile in Figure 3a,b by setting U = 5.7 in eq 6. According to Stein and Chu,[7] the disorder parameter ξ is described by the orientation angle fluctuation of the optical axis within a spherulite. By the model calculation, they suggested that the large ξ results in a broad H_v scattering profile. That is, as ξ increases, the intensity at w = 4 decreases and the intensity decreases more gradually with w. Hence, as a measure of ξ in the radial direction, one can employ the ratio of the intensity at w = 15 to that at w = 4; i.e., $\xi = I(w = 15)/I(w = 4)$. The ξ obtained from Figure 5 is shown in Figure 6a. The disorder parameter slightly decreases with time but never reaches a very low value, suggesting the rodlike H_v pattern should be maintained even at a late stage of crystallization.

The H_v scattering intensity is given by[7]

$$I_{H_v} = {}^1/_2 k' \cos^2\varrho_2 \left(\frac{R}{W}\right)^4 \times \int_{x_1=0}^{w}\int_{x_2=0}^{w} \exp(-|x_{12}|/a')\, J_2(x_1)J_2(x_2)x_1\, dx_1 x_2\, dx_2 \qquad (8)$$

$$\cos\varrho_2 = \cos\theta/(\cos^2\theta + \sin^2\theta \sin^2\mu)^{1/2}$$

where $x = kr \sin\theta$, $k = 2\pi/\lambda$, k' is a proportionality constant, $J_2(x_1)$ and $J_2(x_2)$ are the second-order Bessel functions, $a' = wa/R$, and a is a correlation distance of the ordered region. The $I_{H_v}(w)$ profile in the wide-angle region ($w > 4$) can be calculated for a given parameter a; approximating $J_2(x)x$ is the seven-order polynomial equation. The $I_{H_v}(w)$ curve given for the a value

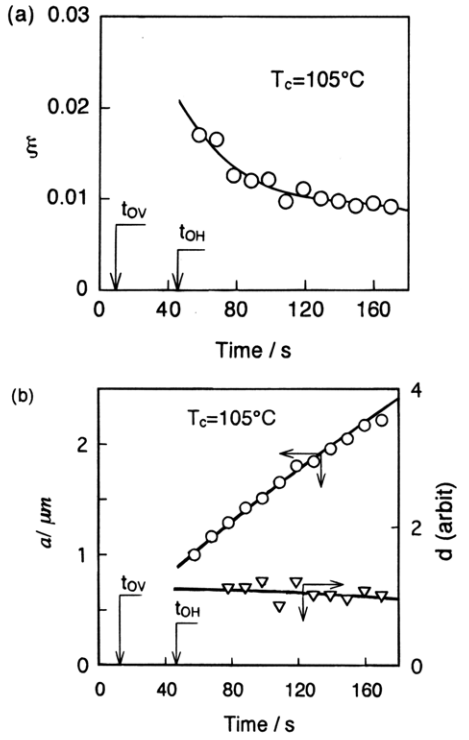

Figure 6. Time variation of (a) the disorder parameter ξ and (b) the correlation distance a and the interfibrile distance d: 30/70 iPP/HSI blend at T_c = 105 °C.

obtained by best fitting to the experimental data is shown by the solid line in Figure 5. The a values thus estimated are shown by the open circles in Figure 6b. The a increases with time. a is related to ξ and the distance between fibrils d:[7]

$$a = d/2\xi^2 \tag{9}$$

The d values estimated by eq 9 are shown as a function of time in Figure 6b. The d is kept almost constant during crystallization. This suggests that new radial fibrils are not formed between the already existing ones. The formation of new fibrils may be restricted due to a high concentration of the impurity (HSI) in the interfibril region. The high concentration of HSI in the interfibril region can be caused by rejection of HSI in fibril order during crystallization of iPP.[8-10] This was supported by the appearance of open spherulites under polarized microscopy.

Figure 7 shows TEM micrographs and their schematic drawings for the blend (a) and for neat iPP (b) both crystallized at T_c = 105 °C. In schematic drawings, the thick and thin stripes represent the radiating primary lamellae and the crosshatch lamellae, respectively. In the micrographs, crystalline lamellae appear as white stripes since the staining agent (RuO_4) penetrates just into amorphous regions. The population of the crosshatch lamellae is low in the blend while it is high in neat iPP. The radiating primary lamellae are arranged parallel to each other in the blend, while they are arranged multidirectionally and are curved in neat iPP. These are consistent with the results of light scattering and polarized optical microscope analyses: the weak positive birefringence spherulite and the rodlike scattering pattern were observed in the blend, in contrast to the strong positive birefringence spherulite and a circular symmetric H_v pattern in neat iPP. That is, in the blend, the weak positive birefringence of the spher-

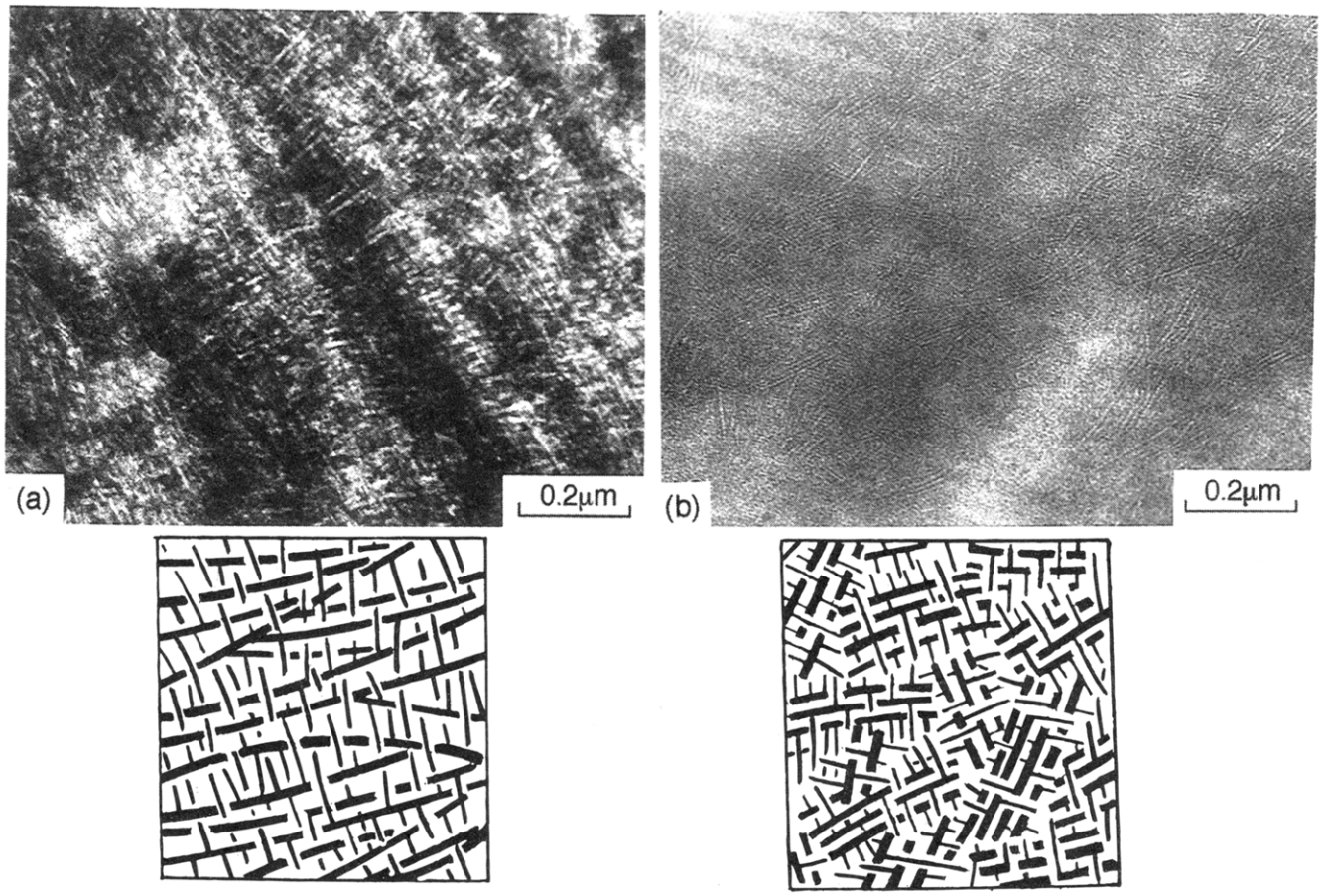

Figure 7. TEM micrographs and schematic drawings: (a) 30/70 iPP/HSI blend and (b) neat iPP, both crystallized at T_c = 105 °C for 1 day.

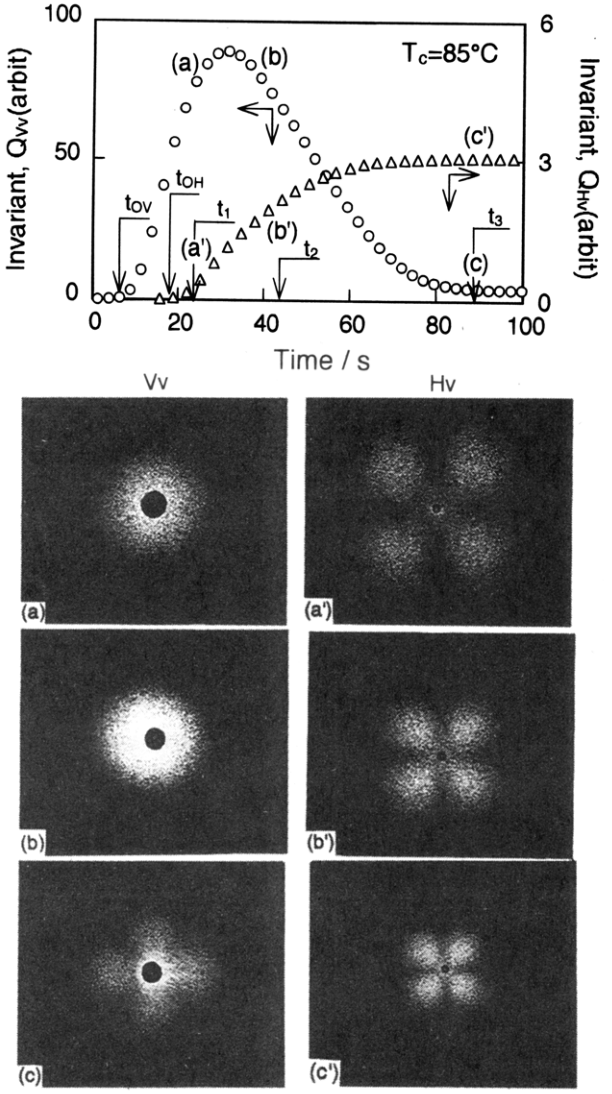

Figure 8. Changes in the invariant and the scattering patterns, both under H_v and V_v modes: 30/70 iPP/HSI blend, T_c = 85 °C. (a, a′) 24, (b, b′) 44, and (c, c′) 88 s.

ulite is ascribed to the low density of the crosshatch lamellae and the rodlike H_v pattern to the parallel arrangement of radiating primary lamellae and the disordered arrangement of crosshatch lamellae.

At lower crystallization temperatures, the situation was very different. Figure 8 shows the change in V_v and H_v scattering patterns from the blends during crystallization at T_c = 85 °C. The V_v pattern changes the shape from a large circular symmetric pattern (a) to a smaller one (b) and then to a cross-shaped one (c) with time. The circular symmetric pattern means no azimuthal angle dependence of the scattered light, implying that the third term in eq 4 is minor ($\alpha_r \approx \alpha_t$). The spherulite with weak negative birefringence observed under the polarized microscope at an early stage suggests $\alpha_t \geq \alpha_r$. It implies that $\alpha_r - \alpha_s$ is comparable to $\alpha_t - \alpha_s$. In such case, the first term in eq 4 is much smaller than the second term, as has been discussed for the V_v patterns at high T_c (Figure 3). Then, the V_v patterns in Figure 8a,b should be ascribed to the second term; however, the value of $\alpha_r - \alpha_s$ should be much smaller than that of the high T_c case in Figure 3 so that the first peak in Figure 3 (ring) could not be detected to render the circular symmetric pattern. The change of the shape from circular symmetric pattern to twofold symmetric with azimuthal dependence can be

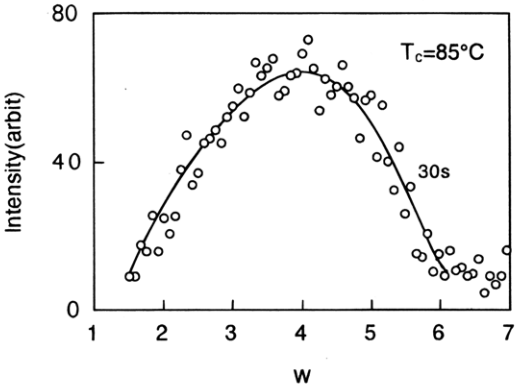

Figure 9. H_v scattering intensity as a function of w. The solid line is a curve calculated by eq 8, setting a = 0.6 μm: 30/70 iPP/HSI blend crystallized at T_c = 85 °C for 30 s.

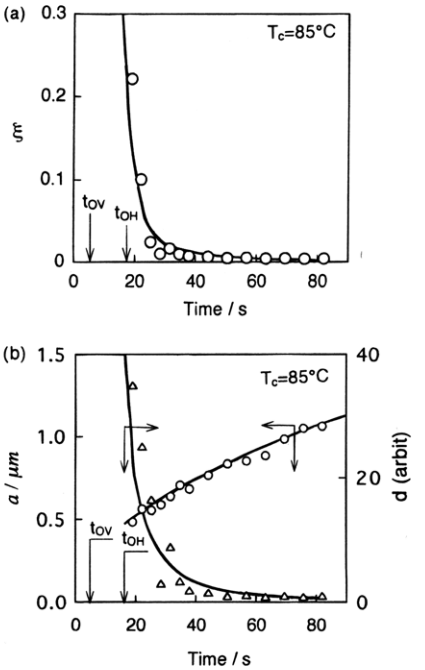

Figure 10. Time variation of (a) the disorder parameter ξ and (b) the correlation distance a and the interfibril distance d: 30/70 iPP/HSI blend at T_c = 85 °C.

interpreted by the increase of the $\alpha_t - \alpha_r$ with time. Actually, the negative birefringence in spherulite became stronger and the H_v intensity increased with time of crystallization.

As shown in Figure 8a′–c′, a four-leaf clover H_v pattern appears and it becomes smaller with time. The appearance of the four-leaf clover pattern is ascribed to high ordering in both tangential and radial directions in the spherulite. The radius of the spherulite can be estimated by the equation of Stein and Rhodes;[11]

$$4.1 = 4\pi(R_s/\lambda)\sin(\theta_m/2) \qquad (10)$$

where θ_m is the scattering angle for the intensity maximum in the one-dimensional scattering profile at μ = 45°. Using the value of R_s given by eq 10, the $I_{H_v}(w)$ profile at μ = 45° is nicely described by eq 8, as shown by the solid line in Figure 9. Following the procedure described above, the values of a, d, and ξ were also calculated. The results are shown in Figure 10. The disorder parameter ξ in radial direction is shown to decrease with time (Figure 10a). The distance d between fibrils decreases rapidly with time and then

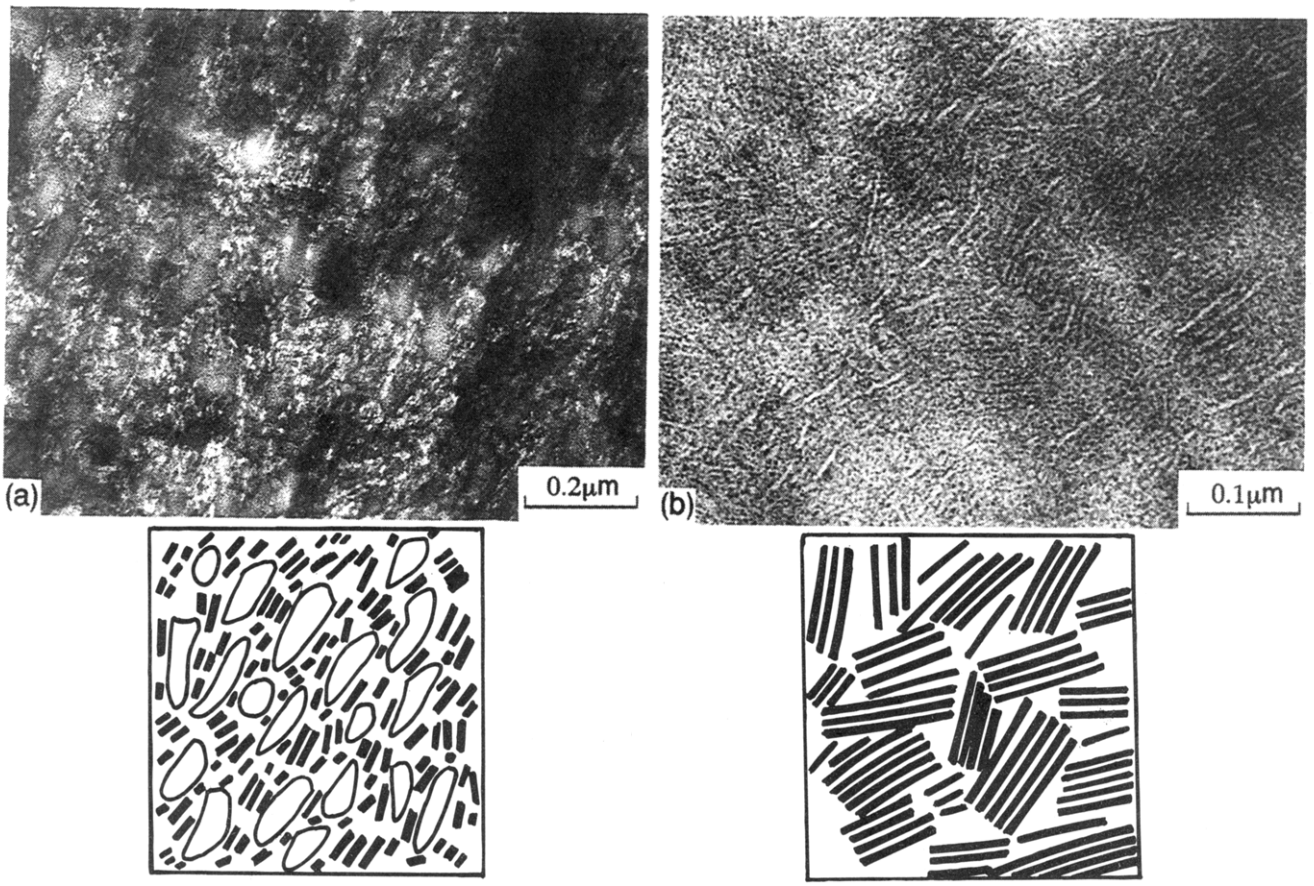

Figure 11. TEM micrographs and schematic drawings: (a)30/70 iPP/HSI blend and (b) neat iPP, both crystallized at $T_c = 85$ °C for 1 day.

levels off (Figure 10b). It suggests that new radiating fibrils are formed between the already existing fibrils during crystallization. The formation of new fibrils could be achieved in the interfibrile region in which HSI concentration is very low. The low HSI concentration may be caused by an entrapment of HSI between lamellar stacks.[8-10]

Figure 11 shows TEM micrographs and their schematic drawings for the blend (a) and for neat iPP (b) both crystallized at $T_c = 85$ °C. No crosshatch lamellae are observed, but fragmented lamellae are seen in the blend. The fragmented lamellae are arranged parallel to each other in a radial direction. Thus, the discussion of light scattering is supported by TEM observation. A white region having a radius of ~0.1 μm is seen. It may be assigned to a HSI-rich amorphous domain between lamellar stacks, supporting the result of light scattering analysis on the entrapment of HSI by segregation between lamellar stacks. It is deduced that the segregated HSI in lamellar scale prevent nucleation on radial primary lamellae so that crosshatching is suppressed. Thus, compared with neat iPP, a unique morphology is available by crystallization from the single-phase mixture of iPP and impurity.

Conclusion

The light scattering and TEM analyses revealed that the new morphologies are available by adding miscible impurity and controlling the T_c. At high T_c, both the population of crosshatch lamellae and the ordering of radial lamellae in the blend are higher than in neat iPP. At low T_c, no crosshatch lamellae are formed but the fragmented lamellae develop in the blend. The fragmented lamellae are arranged parallel with each other in a radial direction.

Acknowledgment. We are greatly indebted to Tsuneo Chiba for the TEM observation.

References and Notes

(1) Khoury, F. *J. Res. Natl. Bur. Stand.* **1966**, *70A*, 29.
(2) Norton, B. R.; Keller, A. *Polymer* **1985**, *26*, 704.
(3) Lee, C. H.; Saito, H.; Inoue, T. *Macromolecules* **1993**, *26*, 6566.
(4) Koberstein, T.; Russell, T. P.; Stein, R. S. J. *Polym. Sci., Polym. Phys. Ed.* **1979**, *17*, 1719.
(5) Yoon, D. Y.; Stein, R. S. *J. Polym. Sci., Polym. Phys. Ed.* **1974**, *12*, 753.
(6) Meeten, G. H. *Optical Properties of Polymers*; Elsevier Applied Science Publishers: London and New York, 1986.
(7) Stein, R. S.; Chu, W. *J. Polym. Sci., A-2* **1970**, *8*, 1137.
(8) Keith, H. D.; Padden, F. J., Jr. *J. Appl. Phys.* **1963**, *34*, 2409.
(9) Keith, H. D.; Padden, F. J., Jr. *J. Appl. Phys.* **1964**, *35*, 1270.
(10) Hudson, S. D.; Davis, D. D.; Lovinger, A. J. *Macromolecules* **1992**, *25*, 1759.
(11) Stein, R. S.; Rhodes, M. B. *J. Appl. Phys.* **1960**, *31*, 1873.

MA950830A